Received October 16, 2019, accepted November 8, 2019, date of publication November 18, 2019,
date of current version November 27, 2019.

Digital Object Identifier 10.1109/ACCESS.2019.2953890

Characterization for the Vehicle-to-Infrastructure Channel in Urban and Highway Scenarios at the Terahertz Band

HAOFAN YI[1,2], (Student Member, IEEE), KE GUAN[1,2], (Senior member, IEEE), DANPING HE[1,2], (Member, IEEE), BO AI[1,2], (Senior Member, IEEE), JIANWU DOU[3], AND JUNHYEONG KIM[4,5]

[1]State Key Laboratory of Rail Traffic Control and Safety, Beijing Jiaotong University, Beijing 100044, China
[2]Beijing Engineering Research Center of High-speed Railway Broadband Mobile Communications, Beijing 100044, China
[3]Wireless Algorithm Department, Product Research and Development system, ZTE Corporation, Shenzhen 518055, China
[4]Moving Wireless Network Research Section, Electronics and Telecommunications Research Institute (ETRI), Daejeon 34129, South Korea
[5]School of Electrical Engineering, Korea Advanced Institute of Science and Technology (KAIST), Daejeon 34141, South Korea

Corresponding author: Ke Guan (kguan@bjtu.edu.cn)

This work was supported in part by the Institute of Information and communications Technology Planning and Evaluation (IITP) Grant Funded by the Korean Government (MSIT) (QoE improvement of open Wi-Fi on public transportation for the reduction of communication expense) under Grant 2018-0-00792, in part by the IITP Grant Funded by the Korean Government (MSIT) (5G AgiLe and fLexible integration of SaTellite And cellulaR) under Grant 2018-0-00175, and in part by the ZTE Corporation.

ABSTRACT With the challenge to form the networks of the Intelligent Transportation Systems (ITS), both technologies of vehicles and wireless communication are required to be connected tightly. In terms of wireless communication, the communication system in the terahertz (THz) frequency range with ultra-large bandwidth is a potential technology to support very high-data-rate wireless transmission at the age of beyond fifth-generation mobile communications (B5G). In this paper, the carrier frequency of 300 GHz with 8 GHz bandwidth vehicle-to-infrastructure (V2I) channel is characterized for the urban and highway scenario, respectively. The self-developed ray-tracing (RT) simulator is employed with the calibrated electromagnetic (EM) parameters. Since the wavelength of carrier frequency approaches the diameters of raindrops and snowflakes, the significant influence of the precipitation on the channel characterization is studied in our work as well. The large-scale parameters of the THz V2I channel, including path loss, Rician K-factor, root-mean-square (RMS) delay spread, and angular spreads are explored in the target scenarios under sunny, rainy, and snowy conditions, respectively. The channel characteristics studied in this paper can be used to support the link-level and system-level design for the future THz vehicular communications.

INDEX TERMS Channel characteristics, ray-tracing simulation, terahertz communication, vehicle-to-infrastructure channel, wave propagation.

I. INTRODUCTION

With the challenge to form internet of intelligent vehicles and with the demand to support high-data-rate communication traffic, the two technologies of vehicles and wireless communications are connected tightly today and also in the future. Intelligent Transportation Systems (ITS) play an important role in the modern transportation field, such as automatic road enforcement, dynamic traffic light sequence, autonomous vehicles, and so on. While the vehicles are in high-speed autonomous model, real-time and fast exchange of dynamic information must be transmitted from vehicle to vehicle (V2V), vehicle to infrastructure (V2I), and vehicle to anything (V2X) in a short time. The V2V communications are realized among the moving vehicles i.e. vehicles act as a source, destination, and router in the communication process. Intermediate nodes (vehicles) transfer messages between source and destination nodes [1]. The V2I communication allows vehicles to communicate with Road Side Units (RSUs), gathering sensing data about the vehicles and sounding traffic [2]. The V2X provides communication services between a vehicle and networks, vehicles, and pedestrians. Such transferred information includes not only small data such as the speed, the location, the directions of

The associate editor coordinating the review of this manuscript and approving it for publication was Xuefeng Yin.

neighboring vehicles, but also the big data such as video of surrounding environments and/or three-dimensional (3D) high-resolution maps [3], which can be used by the transportation control system for congestion avoidance, general warnings (e.g., dangerous situations), and overall traffic efficiency improvement [4]. With the concepts of cloud and fog computing in the future development of the internet of vehicular technology, the whole new security architecture and computing platform for the vehicular network can be achieved [5]. Using the multipath components extracted with the space-alternating generalized expectation-maximization (SAGE) algorithm, the wireless channel response can be characterized from the V2I measurement results [6].

In order to support the potential applications related to the future vehicles, vehicular communications is calling for transmission of a huge amount of data with improved reliability and reduced latency [7]. For the 5th-generation mobile comunications (5G), to improve the spectrum efficiency, millimeter wave (mmWave) band with GHz bandwidth and massive Multiple-Input Multiple-Output (MIMO) [8] are most adopted. At the age of beyond 5G (B5G), the terahertz (THz) frequency range, i.e. beyond 300 GHz, ultra-high bandwidth beyond 20 GHz can be identified, and therefore, over 100 Gbps data rates can be accommodated even only with moderate spectral efficiencies [9].

As the mmWave band has been adopted for consumer electronics, for example, in the 60 GHz unlicensed band the IEEE 802.11ad standard for wireless local area networks supports up to 7 Gb/s data rates [10], most of the existing vehicular works have transferred the target frequency range from sub-6 GHz to mmWave band. In [11], the authors proposed an efficient beam alignment method for mmWave V2I communications leveraging position information and multipath fingerprints. In [12], the communication channel and the self-interference (SI) channel with different settings of transmit-receive antenna spacing and polarization configurations were measured in an indoor environment. In [13], the authors analyzed the suitability of traditional path loss modeling methods for a 28 GHz urban microcell (UMi) environment by using a calibrated ray-tracing (RT) data-set for New York City (NYC). However, in order to support multi-Gbps or even Tbps data rates for intelligent traffic, only the THz bands can provide the multi-gigahertz contiguous bandwidths. For B5G, the THz band is promising to provide the required high capacity, low latency, high reliability, and predictability for safe autonomous driving and ITS needs [4]. In [14], the authors provided an overview to the opportunities as well as the challenges in THz communications for vehicular networks, such as the transceiver design, ultra-massive MIMO antenna arrays, novel waveforms, channel estimation techniques, and so on. Thus, a comprehensive characterization for vehicular communications is required to pave the way of addressing these challenges.

Generally speaking, channel characterization in the THz frequency range has been studied for short propagation distance, mostly in the indoor environment due to the high path loss and atmospheric absorption. The first ultra-wideband (UWB) indoor channel measurement at 300 GHz was in an office environment [15]. The channel modeling document of IEEE 802.15 TG3d [16] describes the propagation characteristics and channel models of the operational environments for the considered application such as close proximity Point-to-Point (P2P) applications [17], intra-device communication [18], backhaul/fronthaul, and data center network [19]. Nie and Akyildiz in [20] presented a three-dimensional (3-D) time-varying THz channel model that captures the peculiarities in propagation parameters in office.

Through the use of array antennas, high-gain and high-directivity beams will be generated to prolong the communication distance. Besides, the maximum communication distance of solid state THz wireless communication system developed by Nippon Telegraph and Telephone Public Corporation (NTT) of Japan is from 3 km to 4 km. However, long distance outdoor communication scenarios at THz band are rarely studied. Due to the longer propagation distance, not only the well-informed atmospheric gas attenuation but also the specific attenuation due to rain and snow cannot be neglected. As for the atmospheric gas attenuation, the main molecules such as water vapor and oxygen molecules are excited by electromagnetic (EM) waves at specific frequencies within the THz band. As a result of the internal vibrations of these molecules, part of the energy of the propagating wave is turned into kinetic energy. The Radiocommunication Sector of the International Telecommunication Union (ITU-R) P.676-11 [21] is given for the estimation of standard atmospheric conditions including oxygen and water vapor molecular at frequencies up to 1000 GHz. In addition, the precipitation attenuation caused by the interaction between the propagating waves and the raindrops and snowflakes has been studied in few experimental studies and limited lectures for the case of outdoor tests in adverse weather conditions which may pose a threat to sensitive measurement equipment. S.Ishii et al. in [22], [23] calculated the rain attenuation at 313 GHz under a rainfall rate of up to 12 mm/h and at 355.2 GHz under a rainfall intensities up to 25 mm/h, where it was found that the prediction of ITU-R P.838-3 [24] has a good agreement with the results of these propagation experiment. In [25], the authors concluded that the rain attenuation of the THz wave increases with the increasing rainfall intensity, and the temperature has little effect on the rain attenuation. In [26], an outdoor line-of-sight (LOS) data link was measured in a significant snowstorm. The excess attenuation caused by snow can be separated into the effects of absorption and scattering throughout the THz range. However, most of these related works only focused on the received power, but not other channel parameters.

Thus, in this paper, we characterize the V2I channel at the THz band comprehensively with the following contributions:

- We reconstruct the urban and highway scenarios and conduct the simulations using the measurement-validated RT simulator with different heights of

transmitter (Tx) and a moving receiver (Rx) carried by a bus. As the wave length at 300 GHz approaches the diameters of raindrops and snowflakes, the significant influence of rain and snow particles cannot be neglected anymore. Thus, we firstly add the attenuation caused by rain and snow to each ray from the simulation results of the V2I channel. In this way, the V2I channel can be studied at 300 GHz for urban scenario and highway scenario under sunny, rainy, and snowy conditions, respectively.

- Based on extensive RT simulation results, the V2I channel in the urban and highway scenarios are characterized in terms of path loss, shadow fading, Rician K-factor, root-mean-square (RMS) delay spread, azimuth angular spread of arrival/departure (ASA/ASD), elevation angular spread of arrival/departure (ESA/ESD). Through analyzing these parameters, we evaluate the Tx heights and reveal the significance of the strong reflection at the THz band. These parameters will provide the fundamental for designing THz technologies and communication systems in a similar scenario under different weather conditions.

The rest of this paper is organized as follows: Section II describes our previous work about the channel sounding measurements in a train test center at 300 GHz for the calibration of the relevant materials and validation of the RT simulator. Section III introduces the urban and highway scenarios and simulation configurations. Section IV details the attenuation caused by raindrops and snowflakes in our study. In Section V and Section VI, all the V2I channel parameters are characterized and summarized for the urban scenario and the highway scenario, respectively. Finally, conclusions and future work are drawn in Section VII.

II. PRELIMINARIES

In our previous study [27], the channel measurement campaigns were supported by an ultra-wideband (UWB) channel sounder at the measured frequency band from 300 GHz to 308 GHz. Two groups of measurements were conducted in a train test center with trains, tracks, and lampposts, including the materials of metal, glass, brick, and so on. The measurement environment and geometry information can be found in Fig. 1 and Fig. 2, respectively. Based on the measured channel gain, the RT is utilized to validate the geometry and to calibrate the EM parameters of related materials. The RT simulator employed in this study is self-developed by Beijing Jiaotong University and Technische Universität Braunschweig. It is composed of a V2V RT simulator [28], [29] and an UWB THz RT simulator [30], [31]. It has been successfully applied in different works [32], [33]. Recently, this RT simulator is extended to a high-performance computing (HPC) cloud-based platform (CloudRT). More details of this platform can be found in [34] as well as the website http://raytracer.cloud.

The power domain mean error of the multipaths in the first measurement compared to the RT simulation results is

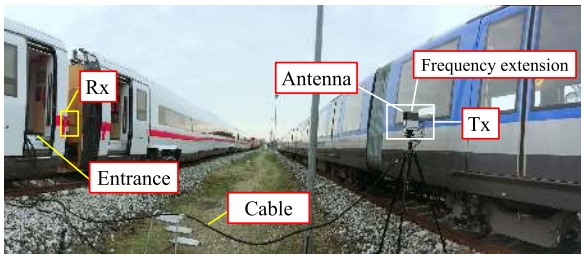

FIGURE 1. Measurement campaign in the train test center at 300 GHz.

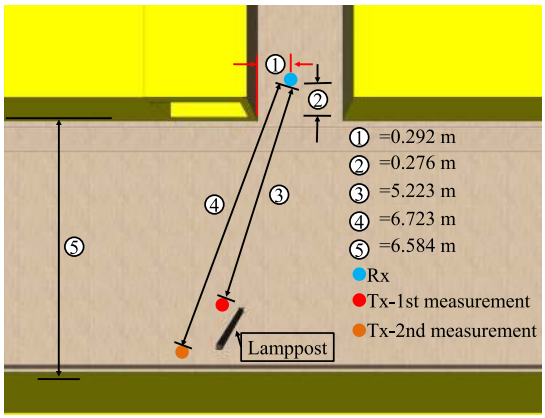

FIGURE 2. Geometry information of the measurement campaign.

TABLE 1. EM parameters of different materials in RT simulations.

Material	Metal	Brick	Glass
ε_r'	1.000	3.026	6.760
ε_r''	1.0E+7	0.159	0.442
S	0	0.0015	0.0030
α	0	40	9

only 0.74 dB, and its time delay mean error is 0.19 ns corresponding to 6 cm in distance. For the second measurement, the mean error in power is 0.4 dB and the mean error in time delay is 0.05 ns. It is noteworthy, there is no error for the LOS path, because it serves as the reference for comparison. The EM parameters of the related materials are listed in Table 1, where ε_r' and ε_r'' represent the real and imaginary parts of the relative permittivity [35], respectively, and where S and α are the scattering coefficient and exponent referring to [36], can be used as the EM parameters in this following study. Furthermore, from the measurement and RT results, it can be observed that the metallic wagon body is the main reflectors in the measured scenario, and therefore, the objects which have a strong influence on the THz propagation channel in our following work should be revealed.

III. RT SIMULATION FOR THZ CHANNEL IN URBAN AND HIGHWAY SCENARIOS

In this section, the simulation scenarios of urban and highway are defined and reconstructed. Totally 8 cases are simulated (sampling interval: 1.38 m in the urban scenario and 1.17 m in the highway scenario, respectively). Moreover, we consider

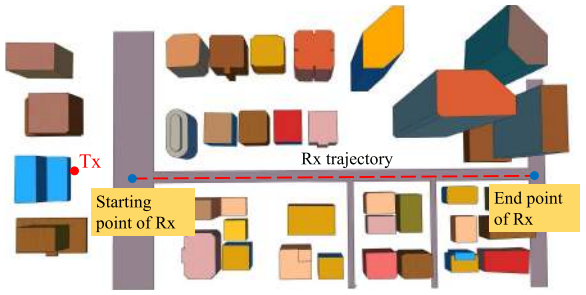

FIGURE 3. 3D model of the constructed urban scenario.

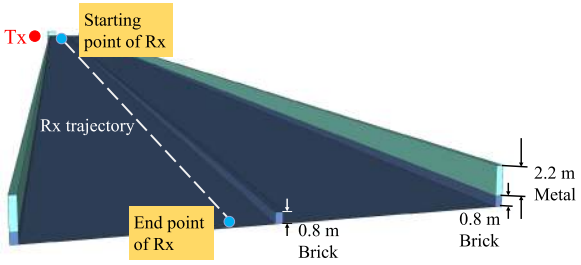

FIGURE 4. 3D model of the constructed highway scenario with metallic barriers.

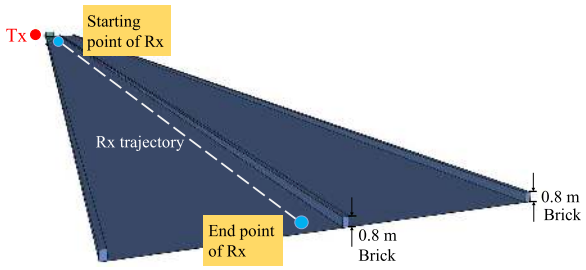

FIGURE 5. 3D model of the constructed highway scenario without metallic barriers.

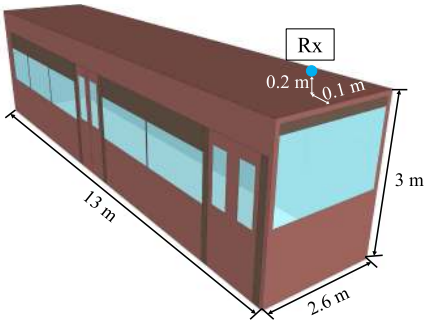

FIGURE 6. Constructed bus and Rx location.

the impact on different weather conditions: sunny, rainy, and snowy days, respectively. The simulation results support the channel characterization and the simulation configurations are detailed as follows.

A. OVERVIEW OF SCENARIOS AND SIMULATION CONFIGURATIONS

In this study, the RT simulations are realized by the constructed 3D environment model with previous calibrated EM parameters. The 3D details of the considered environment are built based on the OpenStreetMap (OSM), which is a collaborative project to create a free editable map of the world. In order to make it easier to access OSM data, a plugin for SketchUp is developed, which can be found on the website http://raytracer.cloud/software. As shown in Fig. 3, 3D urban scenario with 4 lanes is selected as one of the target simulation scenarios. Moreover, an 8-lane highway reconstructed by SketchUp, with a median strip in the middle of the highway. As metal is a type of perfect electric conductor (PEC), on the one hand, the region without LOS but with the reflected path from metallic smooth surface will be promised to build the link through reflection in the even Non-LOS (NLOS) region or strengthen the robustness of communication links and improve the quality and received power. On the other hand, the strong reflected path will cause interference, or it will result in different channel characteristics. For this reason and the reality of highway structure, the constructed highway scenario is divided into two cases with metallic noise barriers (Fig. 4) and without metallic noise barriers (Fig. 5) on the two sides of the road.

In this study, either Tx or Rx antenna is omni-directional vertically polarized antenna with the transmitting power of 0 dBm and with the antenna gain of 0 dBi, in order to simulate the pure propagation channel without the influence of certain antenna pattern. In reality, if the target distance is over 100 meters, then for sure the directional antennas or beamforming techniques will be required. Hence, in the future various antenna patterns or beamforming strategies can be evaluated through coupling them with such a propagation channel based on our study. As shown in Fig. 6, the Rx antenna is carried by a typical bus both in urban and highway scenarios, respectively. The bus is with a length of 13 m, a width of 2.6 m, and a height of 3 m. The antenna is with a height of 0.2 m over the top of the bus and a distance from the bus tail of 0.1 m. The trajectories of Rx and the locations of Tx in our study are shown in Fig. 3, Fig. 4 and Fig. 5, respectively. The travel distance of Rx is 500 m for both scenarios. For the urban scenario, the Tx is placed at the side of the building with a height of 25 m or a traffic light with a height of 5 m, respectively, while three different heights of Tx in the highway scenario are 5 m, 10 m, and 25 m.

The carrier central frequency of simulation is 304 GHz with a bandwidth of 8 GHz. In order to decide the highest effective order of reflected rays which should be traced in simulation, the preliminary simulation along the Rx trajectory is made. As an example, Fig.7 shows the channel gain of the combinations of the ''LOS'' propagation mechanism and different orders of reflection. It is noticeable that the channel gain varies obviously from ''LOS'' to ''LOS+Ref∼2nd Ord'', while it almost does not change from ''LOS+Ref∼2nd Ord'' to ''LOS+Ref∼4th Ord''. Hence, up to the second order of reflected rays should be traced in simulation. The EM properties of materials have been calibrated in our preliminary work in [27] and are listed in Table 1. More details about the simulation configuration are summarized in Table 2.

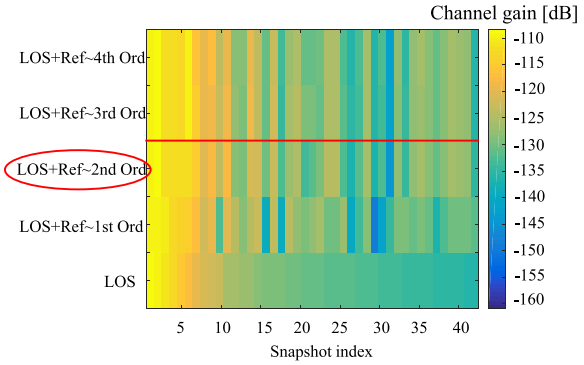

FIGURE 7. Received power of different combinations of rays in the highway scenario.

TABLE 2. Simulation configuration for urban and highway simulations.

Scenario	Urban	Highway
Tx height	5 m, 25 m	5 m, 10 m, 25 m
Antenna type	Omni-directive antenna	
Polarization	Vertical-vertical polarization	
Antenna gain	0 dBi	
Tx power	0 dBm	
Rx height	3.2 m	
Frequency range	300 GHz - 308 GHz	
Frequency point	3200	
Power threshold	50 dB	
Propagation mechanism	LOS+up to 2nd order of reflection+scattering	

In total, 2 cases of urban channel, 6 cases of highway channel are defined, simulated and characterized, respectively. In summary, 8 cases are defined as follows:

1) Urban-5: Tx is 5 m high in the urban scenario.
2) Urban-25: Tx is 25 m high in the urban scenario.
3) Highway-5-Barrier: Tx is 5 m high in the highway scenario with metallic barriers at two sides of the road.
4) Highway-5-noBarrier: Tx is 5 m high in the highway scenario without metallic barriers.
5) Highway-10-Barrier: Tx is 10 m high in the highway scenario with metallic barriers at two sides of the road.
6) Highway-10-noBarrier: Tx is 10 m high in the highway scenario without metallic barriers.
7) Highway-25-Barrier: Tx is 25 m high in the highway scenario with metallic barriers at two sides of the road.
8) Highway-25-noBarrier: Tx is 25 m high in the highway scenario without metallic barriers.

IV. RAIN AND SNOW ATTENUATION

As the wavelength of carrier frequency approaches the diameter of raindrops or snowflakes, the significant influence of these two precipitation on the transmission of high-frequency signals has been recognized for some time. Due to the Mie scattering effect [37], not only the link budget calculation but also the channel parameters are expected to become different. Since the Mie scattering happens when the size of the scatter is nearly equal to the wavelength of the incident light, the influence of raindrops and snowflakes on channel characterization are studied in our work, respectively.

A. RAIN ATTENUATION

The measurements of rain attenuation in [22], [23] indicate that the propagation experiment is in very good agreement with the calculation from the specific attenuation model for use in prediction method by ITU-R P.838-3 [24]. In addition, it can be concluded that the rain attenuation of THz wave is little affected by temperature. The specific rain attenuation γ_{Rain} is predicted at a given rain rate R with the unit of mm/h increases exponentially up to the critical frequency, both for light rain and for heavy rain, which is according to the following relationship:

$$\gamma_{Rain} = kR^{\alpha} \tag{1}$$

where k and α are the functions of the carrier frequency f in the range from 1 GHz to 1 THz and other parameters, such as temperature, polarization direction, and path elevation angle. In our work, the operating carrier frequency is $f = 300$ GHz and the corresponding parameters k and α are calculated according to [24]. As we know, heavy rain in the south of China, especially in the summer, often makes traffic rampant, and tens of thousands of citizens are stranded on the way. As an example, we choose the city, Guangzhou, China, as the research target. The website https://www.latlong.net/ provides the exact latitude and longitude information and with the help of ITU-R P.837-7 [38], an estimate can be obtained from the map of rainfall rate $R_{0.01} = 83.50\ mm/h$, where $R_{0.01}$ is the value which the rainfall rate exceeded for 0.01% of an average year. Thus, the rain attenuation can be calculated for each ray in our study. Although the rain attenuation γ_{Rain} is related to the elevation angle of each path, the values vary little from 26.01 dB/km to 26.21 dB/km while the elevation angle varies from 0° to 180° in our study.

B. SNOW ATTENUATION

Snowflakes have open structures with uneven surfaces and are formed in various shapes: columnar, needle-like, dendritic crystal, etc. The sizes of snowflakes generally vary between 2 mm to 5 mm and their maximum size can reach up to 15 mm [39]. The snowflake has a structure of the combination of air, ice, and water. The attenuation by snowflakes is expected to be more pronounced at a shorter wavelength, such as at 300 GHz band and higher frequency band. In [40], it concludes that three times greater attenuation can be caused by wet snow compared with the same rate of rain precipitation. This can be explained by lower fall velocity and larger size of snow particles compared to raindrops. The general conclusion is that as snowfall rate increases, the attenuation also increases for both wet and dry snowstorms. Higher attenuation is expected for snow particles with higher water content.

Yet, till now few experimental studies on snow effect to the wireless channel have been reported systematically compared to the rain effect on the wireless communication links, not to mention in the THz band range. There is no recommendation in ITU to model the attenuation caused by snow particles. In this study, we refer to the measurement results in the

representative article [26], because the measured LOS link was under the condition of the most significant snowstorm and had the most attenuation among the relevant research and measurements. The measured values of snowflakes are with the rate of 3.5 mm/h and the density of 0.52 g/cm^3 in that study. At 300 GHz, the predicted worst-case attenuation is closed to 2.8 dB for a distance of 8 m in a LOS link, where the Tx was placed under an overhanging roof and the beam propagated through the snowfall to the Rx directly. Hence, in our study, the value of snow attenuation γ_{Snow} is 2.8 dB/8 m, i.e., 350 dB/km for each ray.

C. ADDING THE ATTENUATION TO EACH RAY

In the following work, we aim to emphasize the influences of raindrops and snowflakes. We add the rain attenuation to each ray in line with their elevation angle and path length and calculate the snow attenuation for each ray in line with their path length. As to the best of our knowledge, there is no research on the phase shift after propagating through rain and snow, we assume that the raindrops and snowflakes do not change the phase of each ray, but only cause the attenuation in power domain, namely the amplitude of electric field strength. The calculation process is as follows:

$$P_i = 20\log_{10}\left|E_i e^{j\varphi_i}\right| \tag{2}$$

$$P_{Att,i} = P_i - \gamma \cdot d_i \tag{3}$$

$$\overrightarrow{E_{Att,i}} = E_{Att,i} \cdot e^{\varphi_i} = 10^{P_{Att,i}/20} \cdot e^{j\varphi_i} \tag{4}$$

where P_i is the power of ith ray; E_i and φ_i denotes the electric field amplitude and the phase of each ray; γ is the corresponding unit length attenuation [dB/km]; d_i is the travel distance of each ray; $P_{Att,i}$ is the attenuated power; $\overrightarrow{E_{Att,i}}$ is the attenuated electric field vector, which contains the attenuated electric field amplitude $E_{Att,i}$ and the previous phase φ_i.

V. CHARACTERIZATION OF V2I CHANNEL IN URBAN SCENARIO

Based on the extensive RT simulation results, we firstly make the comprehensive characterization for the V2I channel in the urban scenario with two heights of Tx. The channel characteristics include path loss, shadow fading, RMS delay spread, Rician K-factor, and angular spreads. All these channel parameters are fitted by the normal distribution with the mean value and standard division. Generally, the simulation configuration for THz wireless communication does not include the effect of rain caused attenuation, not to mention the snow attenuation, but only the specific attenuation due to atmospheric gases. Or, most of the work related to rain and snow attenuation only considers the impact on the received power. Hence, in our work, by considering the two weather conditions and the attenuation to each ray, we can separate the simulations results into sunny, rainy, and snowy cases and extract the channel parameters accordingly. All the extracted parameters are summarized in Table 3, where μ_{DS}, μ_{KF}, μ_{ASA}, μ_{ASD}, μ_{ESA}, μ_{ESD} are the mean values of delay spread, K-factor, ASA, ASD, ESA, ESD, respectively.

TABLE 3. Channel characterization for urban scenario.

Channel	Urban scenario					
Case	Urban-5			Urban-25		
Weather	Sunny	Rainy	Snowy	Sunny	Rainy	Snowy
A	21.46	37.83	239.47	21.82	38.36	241.21
B	79.64	47.90	-342.90	76.21	44.10	-349.58
σ_{SF} [dB]	4.52	4.53	12.36	5.71	6.04	13.98
μ_{KF} [dB]	7.32	7.41	8.36	-0.04	0.06	0.80
σ_{KF} [dB]	7.58	7.56	7.61	6.45	6.38	6.44
μ_{DS} [ns]	7.97	7.60	4.91	26.62	23.08	5.29
σ_{DS} [ns]	13.22	11.89	5.47	27.51	23.11	3.94
μ_{ASA} [°]	46.46	45.16	30.38	47.55	46.27	35.27
σ_{ASA} [°]	63.11	61.73	44.06	44.87	43.92	34.42
μ_{ASD} [°]	33.63	33.58	32.75	19.00	16.60	3.18
σ_{ASD} [°]	16.20	16.18	15.82	13.58	11.86	2.11
μ_{ESA} [°]	0.47	0.47	0.47	4.92	4.91	4.91
σ_{ESA} [°]	0.79	0.79	0.78	3.31	3.31	3.40
μ_{ESD} [°]	0.31	0.31	0.31	0.66	0.64	0.61
σ_{ESD} [°]	0.52	0.51	0.51	0.41	0.40	0.37

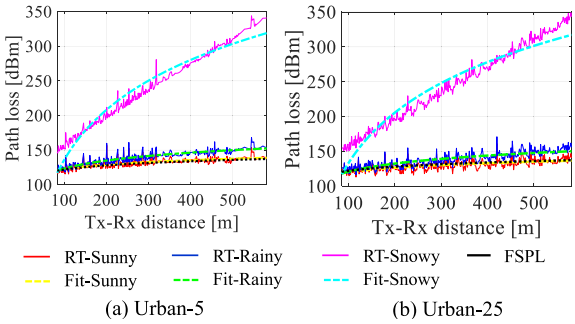

FIGURE 8. Path loss in the urban scenario with different heights of Tx.

σ_{SF}, σ_{DS}, σ_{KF}, σ_{ASA}, σ_{ASD}, σ_{ESA}, σ_{ESD} are the standard deviations of shadow fading, delay spread, K-factor, ASA, ASD, ESA, ESD, respectively. These channel parameters will be discussed below separately.

A. PATH LOSS

In this study, the "A-B" model is used to fit the path loss:

$$PL = A\log_{10}(d) + B + X_\sigma \tag{5}$$

where PL is short for path loss, d is the distance between the Tx and the Rx, A is the slope, B is the intercept, and X_σ is the shadow fading, which can be expressed as a Gaussian variable with zero mean value and a standard deviation of σ_{SF}. Fig. 8 shows the RT and fitting results of path loss for the two heights of Tx, respectively. The results of A and B for sunny, rainy, and snowy conditions in the urban scenario imply a similar path loss at each of the corresponding propagation weather conditions and Tx deployments. As compared between Fig. 9 and Fig. 10, apart from the LOS, there are more strong reflections from the buildings and even the traffic signs in the case of "Urban-25". This leads to the more fluctuant path loss when Tx is 25 m high, which means that more multipaths cause coherent superposition in the propagation process.

By assuming the limited transmission, the communication range will be limited in a short distance. As mentioned in [41], the appropriate frequency band should be determined by the target propagation distance. The maximum distance can be

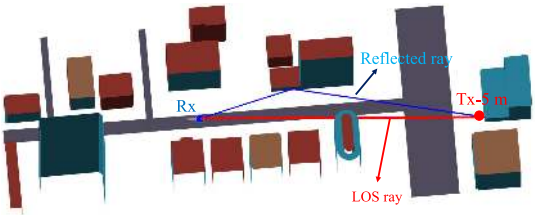

FIGURE 9. One snapshot of the simulations in Urban-5.

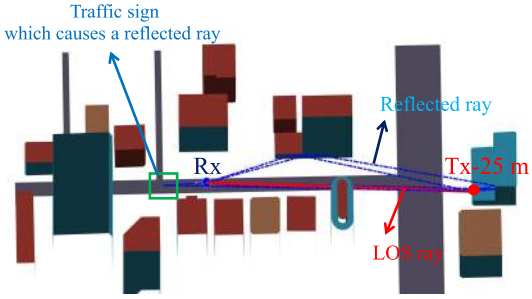

FIGURE 10. One snapshot of the simulations in Urban-25.

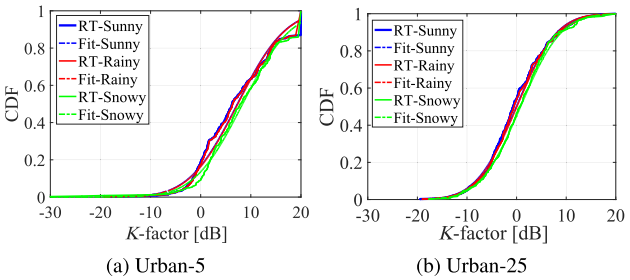

FIGURE 11. *K*-factor in the urban scenario with different heights of Tx.

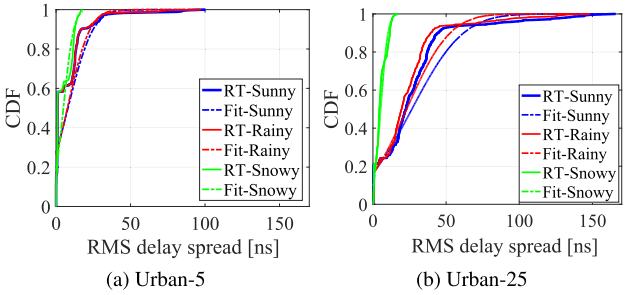

FIGURE 12. RMS delay spread in the urban scenario with different heights of Tx.

1 km when the carrier frequency up to 350 GHz. Besides the free space path loss (142 dB/km), there exists an excess atmospheric absorption attenuation of 9 dB/km at 350 GHz. Hence, the corresponding maximum path loss, where the wireless link can still work, can be approximately 150 dB. Hence, it is noteworthy that in the snowy weather condition, A is to be very large and B becomes to be negative numbers. It means that in the case of snow, the propagation distance is indeed very limited, wherein the "Urban-5" case, the path loss is already 145.7 dB at the beginning of the moving route with a distance of 85 m between Tx and Rx. Hence, the ultra-high-gain directional antenna is suggested in the THz communication when the propagation distance is over 100 m under snowy condition.

B. RICIAN K-FACTOR AND RMS DELAY SPREAD

Since the RT simulator is not bandwidth limited, the K-factor can be directly obtained from its definition - the ratio between the power of strongest ray (which is the LOS path under LOS condition or the strongest multipath under NLOS condition) and the sum of the rest paths. Hence, it can be calculated by the equation:

$$KF = 10 \cdot \log_{10} \frac{\left|E_1 e^{j\varphi_1}\right|^2}{\left|\sum_i^n E_i e^{j\varphi_i} - E_1 e^{j\varphi_1}\right|^2} \tag{6}$$

where KF is short for K-factor, E_i and ϕ_i denote the electric field amplitude and the phase of each ray, respectively. i is the index of each ray, n is the number of rays, and $E_1 e^{j\varphi_1}$ represents the electric field vector of the strongest ray.

In addition, the RMS delay spread for the delay time extent is one of the primary parameters in a multipath radio channel. It is defined in [42], namely the square root of the second central moment of the power delay profile (PDP) by the following equation:

$$\sigma_\tau = \sqrt{\frac{\sum_{n=1}^{N} \tau_n{}^2 \cdot P_n}{\sum_{n=1}^{N} P_n} - \left(\frac{\sum_{n=1}^{N} \tau_n \cdot P_n}{\sum_{n=1}^{N} P_n}\right)^2} \tag{7}$$

where σ_τ denotes the RMS delay spread, P_n and τ_n denote the power and the excess delay of the n-th multipath, respectively.

Fig. 11 shows the K-factor and the fitting results, while Fig. 12 shows the RMS delay spread and the fitting results for 5-m-high Tx and 25-m-high Tx, respectively. When the Tx height is 5 m on the sunny day, the mean value of K-factor is 7.32 dB and the mean value of delay spread is 7.58 ns, respectively. As the Tx height increases to 25 m, the K-factor decreases to -0.04 dB and the delay spread is to be 26.62 ns. This comparison indicates that there are more effective multipaths components (MPCs), as the power threshold is set to be 50 dB, reflected and scattered from the building surface. In addition, in the simulation result of "Urban-5" there is one special snapshot, in which the direct path is blocked by a traffic sign. The traced rays in this snapshot consist of 11 reflected rays with comparable power. This is the reason why the minimum value of K-factor in the case of "Urban-5" is less than -25 dB. Furthermore, it is noteworthy that the reflected path from the traffic sign would not appear when Tx is 5 m high as compared between Fig. 9 and Fig. 10. The authors of [43] characterized the V2X channel in a similar urban scenario with a Tx height of 5 m at 28 GHz, in which the mean values of K-factor and delay spread are 8.82 dB and 9.33 ns, respectively, which are very close to the parameters extracted from our simulation results.

This indicates that the channel propagation characterization is quite influenced by the transceiver's location, although they are jointly determined by the carrier frequency, frequency bandwidth, and propagation region.

Compared with the realistic modern urban scenario, the office buildings are covered with smooth glass mostly. Hence, the strong reflection will happen and our simulation results also confirm this point. This gives a good inspiration for the future use of new materials as reflectors when the LOS path is blocked. Reconfigurable intelligent surface (RIS) [44] and all-dielectric magnetic mirror [45] will be the potential technology from the idea of strong reflection.

As far as either in the rainy or snowy condition, because the reflected rays and scattered rays travel through longer distance compared with the LOS path, they suffer more attenuation than the LOS path. Therefore, in rainy and snowy conditions of each case, the values of K-factor become larger and the values of delay spread become smaller. Mean values of K-factor vary from 7.32 dB to 8.36 dB when Tx is 5 m high, while mean values of K-factor vary from -0.04 dB to 0.80 dB when Tx locates 25 m high. Mean values of delay spread change from 7.97 ns to 4.91 ns when Tx is 5 m high, while mean values of delay spread change from 26.62 ns to 5.29 ns when Tx is 25 m high.

C. ANGULAR SPREADS

The angular spread defines the distribution of the arrival and departure angles of each ray in 3D environments for the Tx and Rx, respectively. Each ray will be assigned an azimuth angle in the horizontal plane and an elevation angle in the vertical plane. Thus, four values of angular spreads can be calculated as follows:

$$\sigma_{AS} = \sqrt{\frac{\sum_{n=1}^{N} \left(\theta_{n,\mu}\right)^2 \cdot P_n}{\sum_{n=1}^{N} P_n}} \tag{8}$$

where σ_{AS} denotes the angular spread (AS), P_n denotes the power of the n-th multipath, and $\theta_{n,\mu}$ is defined by:

$$\theta_{n,\mu} = \text{mod}\left(\theta_n - \mu_\theta + \pi, 2\pi\right) - \pi \tag{9}$$

where θ_n is the azimuth angle of arrival (AoA)/ azimuth angle of departure (AoD)/elevation angle of arrival (EoA)/ elevation angle of departure (EoD) of the n-th ray. μ_n is:

$$\mu_\theta = \frac{\sum_{n=1}^{N} \theta_n \cdot P_n}{\sum_{n=1}^{N} P_n} \tag{10}$$

The comparison of the sub-figures in Fig.13 shows the impact on the angular spreads because of the different heights of Tx of V2I channel in the urban scenario. Generally speaking, the elevation angular spreads of both departure and arrival are much smaller than the azimuth angular spreads,

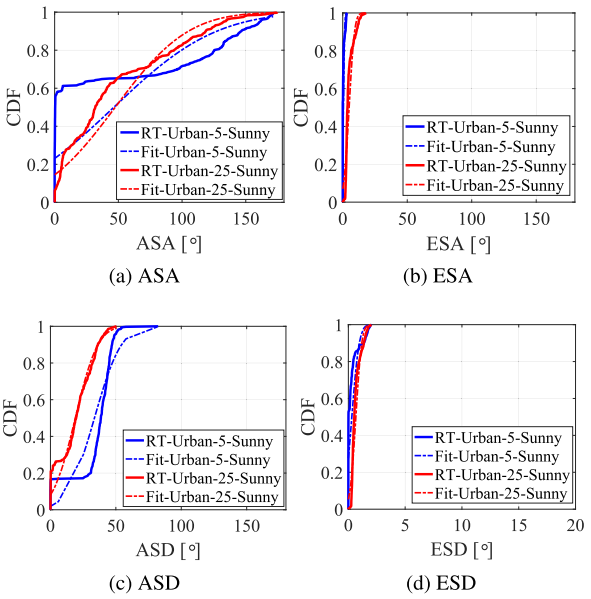

FIGURE 13. Angular spreads in the urban scenario with different heights of Tx.

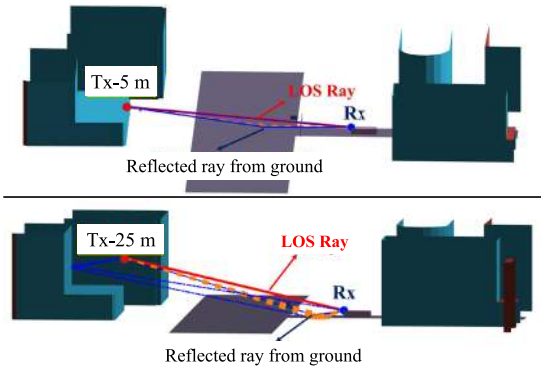

FIGURE 14. Comparison of the same snapshot of the case Urban-5 and Urban-25.

implying that the multipaths come from the horizontal direction mostly. This truthfully responds to the fact that the main objects are located on the two sides of the Rx vehicle in the urban scenario. In addition, as shown in Fig. 14 for 5-m-high Tx and 25-m-high Tx, a ray is reflected from the same point on the ground, implying that the values of ESD and ESA are distributed coincidently in some area. However, as an example shown in Fig. 15, the reflected ray disappears when Tx is 5 m high; while the reflected ray from the ground with a large reflection angle still affects the channel characterization when Tx is 25 high. As can be seen in Fig. 13, the median values of ESA and ESD are almost 0° for 5 m high Tx, which is quite different when Tx is 25 m high.

Regarding the attenuation caused by raindrops and snowflakes, as an example, the mean values of ASA under sunny, rainy, and snowy condition when Tx is 5 m high, are 46.46°, 45.16°, and 30.38°, respectively. The mean values of ESA under the sunny, rainy, and snowy conditions when Tx is 5 m high, are the same with 0.47°, 0.47°, and 0.47°, respectively. Since the effective reflected rays and scattered rays

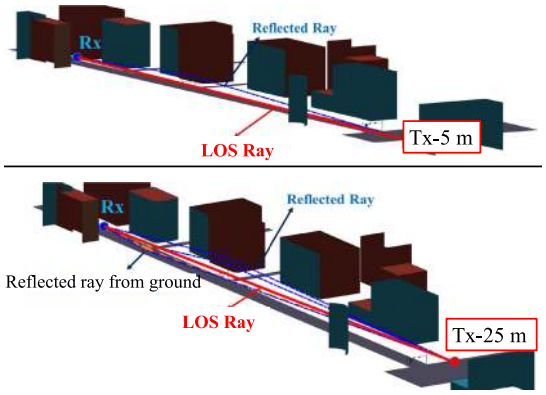

FIGURE 15. Comparison of the same snapshot of the case Urban-5 and Urban-25.

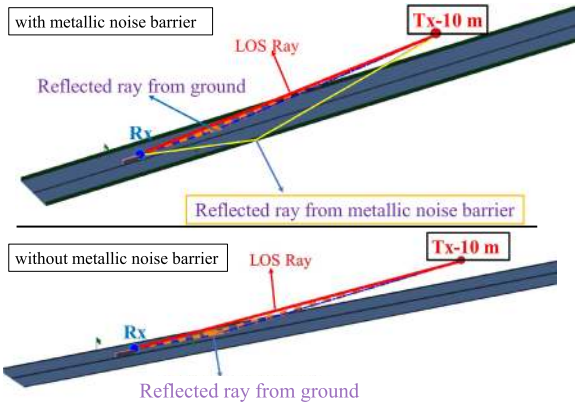

FIGURE 16. Comparison of the same snapshot of the case Highway-10-Barrier and Highway-10-noBarrier.

travel through longer distance, obviously they have higher path loss under rainy and snowy conditions. For the reason that most rays are reflected from the horizontal direction, the ASA and ASD drop sharply compared with each case in sunny condition, while ESA and ESD are almost the same under different weather conditions. Hence, in order to avoid Fig. 13 look messy, we only exhibit the RT results and fitting results in the sunny condition.

VI. KEY CHANNEL PARAMETERS OF V2I CHANNEL IN HIGHWAY SCENARIO

In this part, we make a thorough characterization for three heights (5 m, 10 m, and 25 m) of Tx for the V2I channel in the highway scenario based on the extensive RT simulation results. Furthermore, according to the realistic highway scenario, we divide the highway into two types: with the metallic noise barriers and without the metallic noise barriers (but only a 0.8-m-high brick fence).

From the simulation results, we are surprised to find that the metallic barriers do not affect the channel characteristics when Tx is set to a position of 5 m high or 25 m high. Each ray coming from two sides of the road is reflected from the brick fence, but not from the metallic barriers when Tx is 5 m high. When Tx is 25 m high, the reflected rays come from the ground and the median strip. Hence, for the cases "Highway-5-Barrier", "Highway-5-noBarrier", and "Highway-25-Barrier", "Highway-25-noBarrier", they have the same channel characteristics despite the metallic noise barriers. Yet, when the Tx height is 10 m, the metallic barriers indeed have a great impact on the channel characteristics, where a strong ray is reflected from the barrier, as compared in Fig. 16 for the cases of "Highway-10-Barrier" and "Highway-10-noBarrier".

All the extracted parameters are summarized in Table 4 for "Highway-10-Barrier" and "Highway-10-noBarrier" cases, also including the impact of the raindrops and snowflakes. All the extracted parameters are summarized in Table 5 for "Highway-25-Barrier", "Highway-25-noBarrier", "Highway-5-Barrier", and "Highway-5-noBarrier" cases, including the impact of the raindrops and snowflakes, respectively.

TABLE 4. Characterization for highway scenario when Tx is 10 m high.

Channel	Highway Scenario					
Case	Highway-10-Barrier			Highway-10-noBarrier		
Weather	Sunny	Rainy	Snowy	Sunny	Rainy	Snowy
A	19.15	28.90	149.20	20.19	29.96	150.31
B	83.57	67.85	-126.25	82.30	66.51	-128.02
σ_{SF} [dB]	4.76	4.91	18.46	5.70	5.85	19.00
μ_{KF} [dB]	1.71	1.79	2.46	2.68	2.70	2.82
σ_{KF} [dB]	6.78	6.80	6.76	5.23	5.24	5.25
μ_{DS} [ns]	9.11	8.88	6.65	0.62	0.62	0.61
σ_{DS} [ns]	4.36	4.09	2.29	0.62	0.62	0.62
μ_{ASA} [°]	80.78	78.65	57.33	0.89	0.89	0.87
σ_{ASA} [°]	37.83	37.78	34.88	1.38	1.38	1.35
μ_{ASD} [°]	3.75	3.67	2.84	0.29	0.29	0.29
σ_{ASD} [°]	1.66	1.58	1.03	0.48	0.47	0.47
μ_{ESA} [°]	3.26	3.26	3.20	3.19	3.19	3.19
σ_{ESA} [°]	2.85	2.85	2.86	2.85	2.85	2.87
μ_{ESD} [°]	0.93	0.93	0.94	0.95	0.95	0.95
σ_{ESD} [°]	0.71	0.71	0.73	0.73	0.73	0.74

TABLE 5. Characterization for highway scenario when Tx is 5 m high and 25 m high.

Channel	Highway Scenario					
Case	Highway-25-Barrier Highway-25-noBarrier			Highway-5m-Barrier Highway-5m-noBarrier		
Weather	Sunny	Rainy	Snowy	Sunny	Rainy	Snowy
A	20.56	31.00	115.37	20.66	30.34	149.62
B	81.83	64.46	-149.38	81.08	65.49	-126.45
σ_{SF} [dB]	4.86	5.03	17.26	5.45	5.68	19.38
μ_{KF} [dB]	4.30	4.33	4.62	2.32	2.33	2.41
σ_{KF} [dB]	4.98	4.98	5.01	4.72	4.72	4.76
μ_{DS} [ns]	1.45	1.44	1.42	0.42	0.42	0.39
σ_{DS} [ns]	1.19	1.19	1.16	0.52	0.52	0.49
μ_{ASA} [°]	2.48	2.47	2.37	0.64	0.64	0.61
σ_{ASA} [°]	2.51	2.51	2.41	1.07	1.06	1.04
μ_{ASD} [°]	0.27	0.27	0.26	0.40	0.40	0.39
σ_{ASD} [°]	0.34	0.34	0.32	0.69	0.69	0.67
μ_{ESA} [°]	8.00	7.98	7.84	1.71	1.71	1.71
σ_{ESA} [°]	8.00	7.94	7.87	1.40	1.40	1.39
μ_{ESD} [°]	0.89	0.89	0.87	1.09	1.09	1.08
σ_{ESD} [°]	0.74	0.74	0.72	0.88	0.88	0.88

A. PATH LOSS

Still, the "A-B" model is applied to fit the path loss in the highway scenario. The fitting results are compared in Table 4 and 5. The results of A for sunny, rainy, and snowy conditions in the highway scenario are larger than 20, except for the case "Highway-10-barrier" which is influenced by the metallic noise barriers. The value of A for the case of

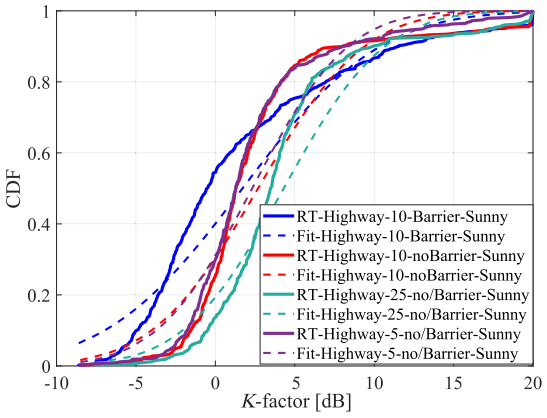

FIGURE 17. Comparison of *K*-factor in highway scenario.

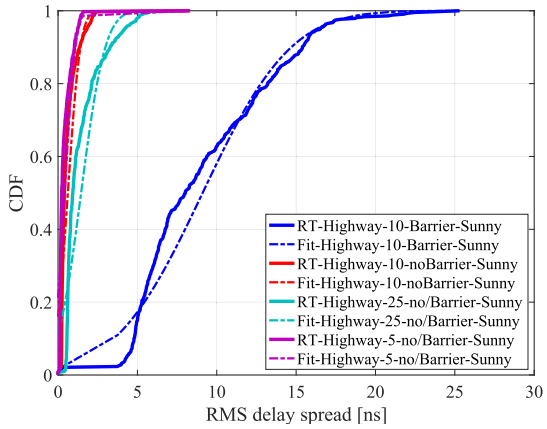

FIGURE 18. Comparison of RMS delay spread in highway scenario.

"Highway-10-barrier" on sunny day is 19.15, which indicates a light waveguide effect caused by multipaths in the highway scenario confined by the metallic barriers.

B. RICIAN K-FACTOR AND RMS DELAY SPREAD

Fig. 17 and Fig. 18 show the comparison of *K*-factor and RMS delay spread for different cases only considering the sunny condition, respectively. In these figures, "Highway-5-no/Barrier" means the combination of the two cases "Highway-5-noBarrier" and "Highway-5-Barrier". In the same way, "Highway-25-no/Barrier" means the combination of the two cases "Highway-25-noBarrier" and "Highway-25-Barrier". The mean values of *K*-factor for "Highway-10-Barrier" and "Highway-10-noBarrier" are 1.71 dB and 2.68 dB, respectively, which indicates that the rays reflected from metallic barriers indeed influence the channel. The mean values of *K*-factor for the 25 m high and 5 m high Tx are 4.30 dB and 2.32 dB, respectively, where the effective reflected rays are from the same material (brick). Based on the geometry of the scenario, the reflected angles of the 25-m-high Tx channel are usually smaller than the 5-m-high Tx channel when the Rx is in the same location.

From the comparison of delay spread, the case of "Highway-10-Barrier" has the largest mean value (9.11 ns) in the time delay domain, which implies that the strong

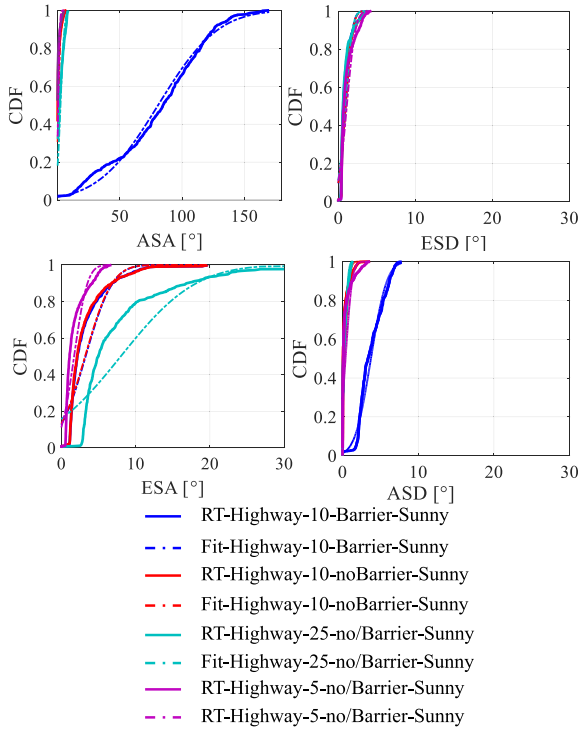

FIGURE 19. Angular spreads in highway scenario with different heights of Tx.

reflected rays also simultaneously travel through longer distances than other reflected rays. Hence, the attenuation caused by raindrops and snowflakes has more impact on this channel. The mean values are 9.11 ns, 8.88 ns, and 6.65 ns in the proper order of sunny, rainy, snowy conditions. However, the influences for other cases due to raindrops and snowflakes can be almost negligible.

C. ANGULAR SPREADS

Fig. 19 shows the influence of the different heights of Tx and with/without metallic noise barriers on the angular spreads. It can be seen clearly that the dark blue lines which represents the case of "Highway-10-Barrier", both in the sub-figures of ASA and ASD, are quite different from other lines. This indicates that the strong reflected rays come from the horizontal direction. The strongly reflected rays can also increase the robustness of the THz wireless link. In addition, this truthfully gives the idea when the Tx is placed at the right height, the reflected ray from the metallic barriers will act as a backup when the direct path is blocked. In the angular domain, all these cases perform similarly, except the case of "Highway-10-Barrier". By considering the rainy and snowy conditions, the variation trend of the angular domain is gradually decreasing as the weather deteriorates, typically for the case of "Highway-10-Barrier".

VII. CONCLUSION AND FUTURE WORK

In this study, to begin with, we recall our previous work about the channel measurements in a train test center at the central frequency of 304.2 GHz with 8 GHz bandwidth as the basis

of this study. Besides the normal sunny condition, since the wavelength of carrier frequency approaches to the diameter of the raindrops or snowflakes, the significance of the influence of these two precipitation on the wireless link cannot be neglected at THz band anymore. The rain attenuation in our study at 300 GHz is in addition related to the elevation angle of each ray, which is ca. 26 dB/km calculated according to ITU-R. P.838-3 [24]. The snow attenuation in our study is 2.8 dB/8 m, correspondingly 348 dB/km. Hence, in the following part, with the help of a self-developed RT simulator, extensive simulations have been done for the V2I channel in two reconstructed urban and highway scenarios considering the sunny, rainy, and snowy conditions, respectively.

In the urban scenario, the path loss for the two heights (5 m and 25 m) of Tx is similar. Meanwhile, the case, where Tx is 5 m high, has smaller RMS delay spread compared to the case where Tx locates 25 m high. When Tx is deployed at the height of 25 m, the reflected paths from buildings or other objects on the two sides of the road can strengthen the robustness of the communication link. Considering the rainy and snowy conditions, it can be concluded that the impact of rain on THz wireless link is limited. Meanwhile, under the snowy condition, the ultra-high-gain directional antenna is suggested in the THz communication when the propagation distance is over 100 m.

At last, the constructed highway scenario is divided into two cases with metallic noise barriers and without metallic barriers on the two sides of the road. The RMS delay spread is quite larger in the case of ''Highway-10-Barrier'' with the mean value of 9.11 ns compared to other cases the values vary from 0.62 ns to 1.45 ns. Since the strong reflected ray is from the side metallic barrier, it affects the ASA (mean value 80.78°) and ASD (mean value 80.78°), where in other cases the mean values of ASAs are from 0.89° to 2.48° and of ASDs are from 0.29° to 0.40°. These channel parameters indicate that the smooth metallic surface indeed affects the channel characteristics if the reflected points locate on the barrier by coincidence.

In summary, snow attenuation and rain attenuation have the greatest impact on path loss generally, and the impact on other channel parameters is relatively small due to the sparsity of THz channel. Metallic surfaces indeed have a great impact on the channel characteristics. THz vehicular links may experience different channel conditions in reality. For example, the signal could be blocked by the front truck. Due to this reason, the LOS communications cannot be guaranteed for the communicating vehicles. From this aspect, this study can pave the fundamental of the future work, where the traffic flow will be under consideration. In addition, the strong reflection from the metallic surface gives a good inspiration for the future use of new materials such can as RIS and all-dielectric magnetic mirrors as reflectors when the LOS path is blocked. Future efforts will be made to involve the Doppler effect to analyze the time-vary channel response in V2I scenarios, and analyze the influence of various antenna patterns or beamforming strategies.

REFERENCES

[1] D. He, L. Wang, K. Guan, B. Ai, J. Kim, and Z. Zhong, ''Channel characterization for mmWave vehicle-to-infrastructure communications in urban street environment,'' in *Proc. 13th Eur. Conf. Antennas Propag. (EuCAP)*, Mar./Apr. 2019, pp. 1–5.
[2] Shivashankar, B. H. Chowdary, G. Kaur, A. Kumari, and C. K. Reddy, ''Design and development of new apparatus in VANETs for safety and accident avoidance,'' in *Proc. IEEE Int. Conf. Recent Trends Electron., Inf. Commun. Technol. (RTEICT)*, May 2016, pp. 1695–1698.
[3] X. Cheng, C. Chen, W. Zhang, and Y. Yang, ''5G-Enabled cooperative intelligent vehicular (5GenCIV) framework: When benz meets marconi,'' *IEEE Intell. Syst.*, vol. 32, no. 3, pp. 53–59, May 2017.
[4] K. M. S. Huq, S. A. Busari, J. Rodriguez, V. Frascolla, W. Bazzi, and D. C. Sicker, ''Terahertz-enabled wireless system for beyond-5G ultra-fast networks: A brief survey,'' *IEEE Netw.*, vol. 33, no. 4, pp. 89–95, Jul./Aug. 2019.
[5] Z. Meng, Z. Guan, Z. Wu, A. Li, and Z. Zhong, ''Security enhanced Internet of vehicles with cloud-fog-dew computing,'' *ZTE Commun.*, vol. 15, no. S2, pp. 43–46, 2017.
[6] T. Domínguez-Bolaño, J. Rodríguez-Piñeiro, J. A. García-Naya, X. Yin, and L. Castedo, ''Measurement-based characterization of train-to-infrastructure 2.6 GHz propagation channel in a modern subway station,'' *IEEE Access*, vol. 6, pp. 52814–52830, 2018.
[7] X. Cheng, R. Zhang, and L. Yang, ''Wireless toward the era of intelligent vehicles,'' *IEEE Internet Things J.*, vol. 6, no. 1, pp. 188–202, Feb. 2019.
[8] J. Chen, X. Yin, X. Cai, and S. Wang, ''Measurement-based massive MIMO channel modeling for outdoor LoS and NLoS environments,'' *IEEE Access*, vol. 5, pp. 2126–2140, 2017.
[9] T. Kürner and S. Priebe, ''Towards THz communications—Status in research, standardization and regulation,'' *J. Infr., Millim., THz. Waves*, vol. 35, pp. 53–62, Aug. 2013, doi: 10.1007/s10762-013-0014-3.
[10] F. Jameel, S. Wyne, S. J. Nawaz, and Z. Chang, ''Propagation channels for mmWave vehicular communications: State-of-the-art and future research directions,'' *IEEE Wireless Commun.*, vol. 26, no. 1, pp. 144–150, Feb. 2019.
[11] V. Va, J. Choi, T. Shimizu, G. Bansal, and R. W. Heath, Jr., ''Inverse multipath fingerprinting for millimeter wave V2I beam alignment,'' *IEEE Trans. Veh. Technol.*, vol. 67, no. 5, pp. 4042–4058, May 2018.
[12] Y. He, X. Yin, and H. Chen, ''Spatiotemporal characterization of self-interference channels for 60-GHz full-duplex communication,'' *IEEE Antennas Wireless Propag. Lett.*, vol. 16, pp. 2220–2223, 2017.
[13] A. Karttunen, A. F. Molisch, S. Hur, J. Park, and C. J. Zhang, ''Spatially consistent street-by-street path loss model for 28-GHz channels in micro cell urban environments,'' *IEEE Trans. Wireless Commun.*, vol. 16, no. 11, pp. 7538–7550, Nov. 2017.
[14] S. Mumtaz, J. M. Jornet, J. Aulin, W. H. Gerstacker, X. Dong, and B. Ai, ''Terahertz communication for vehicular networks,'' *IEEE Trans. Veh. Technol.*, vol. 66, no. 7, pp. 5617–5625, Jul. 2017.
[15] S. Priebe, C. Jastrow, M. Jacob, T. Kleine-Ostmann, T. Schrader, and T. Kürner, ''Channel and propagation measurements at 300 GHz,'' *IEEE Trans. Antennas Propag.*, vol. 59, no. 5, pp. 1688–1698, May 2011.
[16] *TG3d Channel Modeling Document*, document IEEE P802.15, 2016. [Online]. Available: https://mentor.ieee.org/802.15/dcn/14/15-14-0310-18-003d-channel-modeling-document.docx
[17] D. He, K. Guan, A. Fricke, B. Ai, R. He, Z. Zhong, A. Kasamatsu, I. Hosako, and T. Kürner, ''Stochastic channel modeling for Kiosk applications in the Terahertz band,'' *IEEE Trans. THz Sci. Technol.*, vol. 7, no. 5, pp. 502–513, Sep. 2017.
[18] X. Cheng, Y. Li, B. Ai, X. Yin, and Q. Wang, ''Device-to-device channel measurements and models: A survey,'' *IET Commun.*, vol. 9, no. 3, pp. 312–325, 2015.
[19] B. Peng and T. Kürner, ''A stochastic channel model for future wireless THz data centers,'' in *Proc. Int. Symp. Wireless Commun. Syst. (ISWCS)*, Aug. 2015, pp. 741–745.
[20] S. Nie and I. F. Akyildiz, ''Three-dimensional dynamic channel modeling and tracking for terahertz band indoor communications,'' in *Proc. IEEE 28th Annu. Int. Symp. Pers., Indoor, Mobile Radio Commun. (PIMRC)*, Oct. 2017, pp. 1–5.
[21] *Attenuation by Atmospheric Gases*, ITU-Rec. P.676-11, 2016.
[22] S. Ishii, ''Rain attenuation at terahertz,'' *Wireless Eng. Technol.*, vol. 1, pp. 92–95, Oct. 2010.
[23] S. Ishii, S. Sayama, and T. Kamei, ''Measurement of rain attenuation in terahertz wave range,'' *Wireless Eng. Technol.*, vol. 2, no. 3, pp. 119–124, 2011.

[24] *Specific Attenuation Model for Rain for Use in Prediction Methods*, document ITU-Rec. P.838-3, 2005.

[25] Y. Luo, W.-X. Huang, and Z.-Y. Luo, "Attenuation of terahertz transmission through rain," *Optoelectron. Lett.*, vol. 8, no. 4, pp. 310–313, Aug. 2012.

[26] J. Ma, J. Adelberg, R. Shrestha, L. Moeller, and D. M. Mittleman, "The effect of snow on a terahertz wireless data link," *J. Infr., Millim., THz Waves*, vol. 39, pp. 505–508, Jun. 2018.

[27] K. Guan, B. Peng, D. He, J. M. Eckhardt, S. Rey, B. Ai, Z. Zhong, and T. Kürner, "Measurement, simulation, and characterization of train-to-infrastructure inside-station channel at the terahertz band," *IEEE Trans. THz Sci. Technol.*, vol. 9, no. 3, pp. 291–306, May 2019.

[28] K. Guan, Z. Zhong, B. Ai, and T. Kürner, "Deterministic propagation modeling for the realistic high-speed railway environment," in *Proc. IEEE 77th Veh. Technol. Conf. (VTC Spring)*, Dresden, Germany, Jun. 2013, pp. 1–5.

[29] J. Nuckelt, T. Abbas, F. Tufvesson, C. Mecklenbrauker, L. Bernado, and T. Kürner, "Comparison of ray tracing and channel-sounder measurements for vehicular communications," in *Proc. IEEE 77th Veh. Technol. Conf. (VTC Spring)*, Jun. 2013, pp. 1–5.

[30] S. Priebe and T. Kürner, "Stochastic modeling of THz indoor radio channels," *IEEE Trans. Wireless Commun.*, vol. 12, no. 9, pp. 4445–4455, Sep. 2013.

[31] K. Guan, B. Peng, D. He, J. M. Eckhardt, S. Rey, B. Ai, Z. Zhong, and T. Kürner, "Channel characterization for intra-wagon communication at 60 and 300 GHz bands," *IEEE Trans. Veh. Technol.*, vol. 68, no. 6, pp. 5193–5207, Jun. 2019.

[32] K. Guan, B. Ai, B. Peng, D. He, G. Li, J. Yang, Z. Zhong, and T. Kürner, "Towards realistic high-speed train channels at 5G millimeter-wave band—Part I: Paradigm, significance analysis, and scenario reconstruction," *IEEE Trans. Veh. Technol.*, vol. 67, no. 10, pp. 9112–9128, Oct. 2018.

[33] K. Guan, B. Ai, B. Peng, D. He, G. Li, J. Yang, Z. Zhong, and T. Kürner, "Towards realistic high-speed train channels at 5G millimeter-wave band—Part II: Case study for paradigm implementation," *IEEE Trans. Veh. Technol.*, vol. 67, no. 10, pp. 9129–9144, Oct. 2018.

[34] D. He, B. Ai, K. Guan, L. Wang, Z. Zhong, and T. Kürner, "The design and applications of high-performance ray-tracing simulation platform for 5G and beyond wireless communications: A tutorial," *IEEE Commun. Surveys Tuts.*, vol. 21, no. 1, pp. 10–27, 1st Quart., 2019.

[35] L. F. Chen, C. K. Ong, C. P. Neo, V. V. Varadan, and V. K. Varadan, *Microwave Electronics: Measurement and Materials Characterization*. Hoboken, NJ, USA: Wiley, 2005.

[36] V. Degli-Esposti, F. Fuschini, E. M. Vitucci, and G. Falciasecca, "Measurement and modelling of scattering from buildings," *IEEE Trans. Antennas Propag.*, vol. 55, no. 1, pp. 143–153, Jan. 2007.

[37] T. C. Chang, P. Gloersen, T. Schmugge, T. T. Wilheit, and H. Zwally, "Microwave emission from snow and glacier ice," *J. Glaciol.*, vol. 16, no. 74, pp. 23–39, 1976.

[38] *Characteristics of Precipitation for Propagation Modelling*, document ITU-Rec. P.837-7, 2017.

[39] T. Oguchi, "Electromagnetic wave propagation and scattering in rain and other hydrometeors," *Proc. IEEE*, vol. 71, no. 9, pp. 1029–1078, Sep. 1983.

[40] V. W. Richard, J. E. Kammerer, and R. G. Reitz, "140-GHz attenuation and optical visibility measurements of fog, rain and snow," Army Ballistic Res. Lab., Aberdeen Proving Ground, MD, USA, Tech. Rep. ADA051055, 1977.

[41] M. Tamosiunaite, S. Tamosiunas, M. Zilinskas, and G. Valusis, "Atmospheric attenuation of the terahertz wireless networks," in *Broadband Communications Networks-Recent Advances and Lessons from Practice*. Rijeka, Croatia: InTech, 2017.

[42] T. Rappaport, *Wireless Communications: Principles and Practice*, 22nd ed. Upper Saddle River, NJ, USA: Prentice-Hall, 2002.

[43] L. Wang, B. Ai, D. He, K. Guan, J. Zhang, J. Kim, and Z. Zhong, "Vehicle-to-infrastructure channel characterization in urban environment at 28 GHz," *China Commun.*, vol. 16, no. 2, pp. 36–48, Feb. 2019.

[44] C. Huang, A. Zappone, G. C. Alexandropoulos, M. Debbah, and C. Yuen, "Reconfigurable intelligent surfaces for energy efficiency in wireless communication," *IEEE Trans. Wireless Commun.*, vol. 18, no. 8, pp. 4157–4170, Aug. 2019.

[45] Z. J. Ma, S. M. Hanham, P. Albella, B. Ng, H. T. Lu, Y. Gong, S. A. Maier, and M. Hong, "Terahertz all-dielectric magnetic mirror metasurfaces," *ACS Photon.*, vol. 3, no. 6, pp. 1010–1018, May 2016.

HAOFAN YI (S'19) was born in Xianyang, China, in 1993. She received the B.E. degree from Xidian University, Xi'an, China, in 2015, and the M.Sc. degree in electrical engineering from Technische Universität Braunschweig, Braunschweig, Germany, in 2018. She is currently pursuing the Ph.D. degree with Beijing Jiaotong University, Beijing, China. Her research activities are mainly in THz wave propagation and THz channel modeling.

KE GUAN (S'10–M'13–SM'19) received the B.E. and Ph.D. degrees from Beijing Jiaotong University, in 2006 and 2014, respectively.

In 2009, he was a Visiting Scholar with the Universidad Politécnica de Madrid, Spain. From 2011 to 2013, he was a Research Scholar with the Institut für Nachrichtentechnik (IfN), Technische Universität Braunschweig, Germany. From September 2013 to January 2014, he was invited to conduct joint research with the Universidad Politécnica de Madrid, Spain. He is currently an Associate Professor with the State Key Laboratory of Rail Traffic Control and Safety, School of Electronic and Information Engineering, Beijing Jiaotong University. He has authored/coauthored two books and one book chapter, more than 200 journal and conference papers, and four patents. His current research interests include measurement and modeling of wireless propagation channels, high-speed railway communications, vehicle-to-x channel characterization, and indoor channel characterization for high-speed short-range systems, including future terahertz communication systems. Dr. Guan is the Pole Leader of European Railway Research Network of Excellence (EURNEX). He has been a delegate in 3GPP and a member of the IC1004 and CA15104 initiatives. He was a recipient of the 2014 International Union of Radio Science (URSI) Young Scientist Award. In 2015, he was awarded a Humboldt Research Fellowship for postdoctoral researchers. His articles received eight Best Paper Awards, including the IEEE Vehicular Technology Society 2019 Neal Shepherd Memorial Best Propagation Paper Award. He serves as a Publicity Chair in PIMRC 2016, the Publicity Co-Chair in ITST 2018, the Track Co-Chair in EuCNC, the Session Convener of EuCAP 2015-2019, and a TPC Member for many IEEE conferences, such as Globecom, ICC, and VTC. He is an Editor of IEEE Access, *IET Microwave, Antenna and Propagation, Physical Communication*, and a Guest Editor of the IEEE Transactions on Vehicular Technology and the IEEE Communication Magazine.

DANPING HE (M'16) received the B.E. degree from the Huazhong University of Science and Technology, in 2008, the M.Sc. degree from the Universite Catholique de Louvain (UCL) and Politecnico di Torino (PdT), in 2010, and the Ph.D. degree from the Universidad Politécnica de Madrid, in 2014.

In 2012, she was a Visiting Scholar with the Institut National de Recherche en Informatique et en Automatique, France. She was a Research Engineer with Huawei Technologies, from 2014 to 2015. From 2016 to 2018, she conducted Postdoctoral Research at Beijing Jiaotong University, where she is currently an Associate Professor. She has authored/coauthored more than 40 articles, three patents, and one IEEE standard. Her current research interests include radio propagation and channel modeling, ray-tracing technologies, and wireless communication algorithm design. Her articles received five best paper awards. She also received the 2019 Applied Computational Electromagnetics' Society (ACES)-China Young Scientist Award.

BO AI (M'00–SM'10) received the master's and Ph.D. degrees from Xidian University, China. He graduated from Tsinghua University with the honor of Excellent Postdoctoral Research Fellow from Tsinghua University, in 2007. He was a Visiting Professor with the Electrical Engineering Department, Stanford University, in 2015. He is currently a Full Professor and a Ph.D. Candidate Advisor with BJTU. He has authored/coauthored eight books and published over 300 academic research articles in his research area. He holds 26 invention patents. He has been the Research Team Leader for 26 national projects and has received some important scientific research prizes. He has been notified by the Council of Canadian Academies (CCA) that, based on the Scopus database. He has been listed as one of the Top one percent of authors in his field all over the world. His interests include the research and applications of channel measurement and channel modeling, and dedicated mobile communications for rail traffic systems. He is an IET Fellow and an IEEE VTS Distinguished Lecturer. He has received many awards, such as Outstanding Youth Foundation from the National Natural Science Foundation of China, the Qiushi Outstanding Youth Award from the Hong Kong Qiushi Foundation, New Century Talents from the Chinese Ministry of Education, the Zhan Tianyou Railway Science and Technology Award of the Chinese Ministry of Railways, and the Science and Technology New Star of the Beijing Municipal Science and Technology Commission. He has been a Co-Chair or a Session/Track Chair for many international conferences. He is an Editor of the IEEE TRANSACTIONS ON CONSUMER ELECTRONICS and an Editorial Committee member of *Wireless Personal Communications Journal*. He has been the Lead Guest Editor for Special Issues of the IEEE TRANSACTIONS ON VEHICULAR TECHNOLOGY, the IEEE ANTENNAS AND PROPAGATIONS LETTERS, and *International Journal on Antennas and Propagation*.

JIANWU DOU received the Ph.D. degree in robotic mechanism from the Beijing University of Technology, Beijing, China, in 2001.

From 2000 to 2014, he was the Head of Wireless RRM Team, including 2G/3G/4G/WLAN. He was in charge of developing a multi-RAT wireless system simulation platform. From 2012 to 2014, he was the Product Manager of ZTE iNES, a multicell/multi-UE hardware wireless channel emulator. From 2005 to 2017, he was the Vice Director with the Wireless Algorithm Department, ZTE Corporation, Shenzhen, China. He is currently in charge of the National Major Project and participated in two 5G projects supported by the Ministry of Industry and Information Technology of China. His current research interests include 5G/B5G channel modeling, new air-interface, unmanned aerial vehicle, and nonterrestrial network research.

Dr. Dou was a recipient of the Science and Technology Award (1st Level) from the China Institute of Communications, from 2014 to 2015, and the Award for Chinese Outstanding Patented Invention from WIPO-SIPO, in 2011.

JUNHYEONG KIM received the B.S. degree from Tsinghua University, Beijing, China, in 2008, and the M.S. degree from the Korea Advanced Institute of Science and Technology (KAIST), Daejeon, South Korea, in 2011, where he is currently pursuing the Ph.D. degree with the School of Electrical Engineering. Since 2011, he has been with the Electronics and Telecommunications Research Institute, Daejeon. His main research interests include millimeter-wave communications, MIMO, cooperative communications, and handover.